

SiGe BiCMOS Heterodyne Receiver Frontend for Remote Sensing with Small Satellites

Alexandra Glück, Nick Rothbart, Klaus Schmalz, and Heinz-Wilhelm Hübers

Abstract—Molecular spectroscopy with THz heterodyne receivers is an important and widely used method for remote sensing of gases in space, in the Earth’s and planetary atmospheres, as well as in the coma of comets. For the use on small satellites, compact and light-weight receivers are needed. We have developed an integrated SiGe BiCMOS receiver frontend which is tunable from 225 GHz to 255 GHz and have characterized it for heterodyne spectroscopy. The double-sideband noise temperature is 11 000 K at a local oscillator frequency of 240 GHz and the Allan time is 1 s. With this receiver we successfully performed heterodyne absorption and emission spectroscopy of acetonitrile in laboratory experiments.

Index Terms—BiCMOS integrated circuits, heterodyne spectroscopy, millimeter-wave technology, remote sensing, terahertz technology.

I. INTRODUCTION

HETERODYNE spectroscopy in the millimeter-wave (mmW) and terahertz (THz) region is an important tool in space applications due to its capability of sensitive detection of trace gases with high spectral resolution. The identification and quantification of the molecules is based on spectral fingerprints, mainly resulting from rotational transitions. Heterodyne receivers in the mmW/THz range can be used, for example, for the investigation of Earth’s atmosphere to provide information about photochemical processes, pollution, or climate change.

A large variety of trace gases have been detected with high spectral resolution (< MHz) by the Earth Observing System Microwave Limb Sounder (EOS MLS) on the NASA Aura satellite [1]. Among the detected molecules are, for example, carbon monoxide (CO), chlorine monoxide (ClO), sulfur dioxide (SO₂), ozone (O₃), nitrous oxide (N₂O), water (H₂O) and acetonitrile (CH₃CN). Global maps as well as altitude profiles have been obtained from these data. The Earth’s atmosphere has also been studied by the Superconducting Submillimeter-Wave Limb Sounder on the International Space Station [2] or the submillimeter wave radiometer on the Odin satellite [3]. Recently, a THz heterodyne spectrometer has been used for spectrally resolved observations of atomic oxygen

This work was supported by Deutsche Forschungsgemeinschaft (DFG) through the DFG project ESSENCE under Grant SPP 1857.

A. Glück is with the Institute of Optical Sensor Systems of German Aerospace Center (DLR), 12489 Berlin, Germany and the Department of Physics of Humboldt-Universität zu Berlin, 12489 Berlin, Germany (e-mail: alexandra.glueck@dlr.de).

N. Rothbart is with the Institute of Optical Sensor Systems of German Aerospace Center (DLR), 12489 Berlin, Germany.

K. Schmalz was with IHP - Leibniz-Institut für Innovative Mikroelektronik, 15236 Frankfurt (Oder), Germany.

H.-W. Hübers is with the Institute of Optical Sensor Systems of German Aerospace Center (DLR), 12489 Berlin, Germany and the Department of Physics of Humboldt-Universität zu Berlin, 12489 Berlin, Germany

Manuscript received ...; revised

in the mesosphere and lower thermosphere of Earth [4]. MmW/THz heterodyne spectrometers are also valuable for the investigation of planetary atmospheres and comets [5]–[8].

For cost-efficient monitoring of the atmosphere, small satellites are desirable. CubeSats are very small, low cost satellites, which consist of modules with standardized interfaces, each with a volume of $10 \times 10 \times 10 \text{ cm}^3$ and a mass of up to 1.33 kg [9]. By now, thousands of them have been launched successfully, mostly for the purpose of Earth observation [10]. This approach has various advantages over large-scale satellites and is promising for the future as can be seen by the increasing number of CubeSat launches.

There are several receiver technologies for mmW/THz remote sensing in planetary/Earth atmospheric science. GaAs- and InP-based receivers provide the lowest noise temperature ($\approx 1000 \text{ K}$) without cryogenic cooling [11], but this technology lacks the integration capability and therefore systems are discrete or hybrid assemblies. These assembled systems have a large form factor and a rather large weight. Thus, this technology is not ideally suited for the use in nanosatellites such as CubeSats. For the receiver frontend, Si-based technology is well-suited as it offers the perspective for very sensitive low-cost devices with a high integration level. Heterodyne receivers were demonstrated in CMOS as well as SiGe BiCMOS technology [12]–[14]. Sensitive absorption spectroscopy was demonstrated using a SiGe BiCMOS transmitter and receiver [15]. Also, CMOS receiver arrays were reported which are feasible for imaging in the atmosphere [16]. It is important to note that compact backend spectrometers suitable for this application have already been successfully demonstrated [11], [17].

In this paper, we report on the performance of a SiGe BiCMOS based heterodyne receiver operating in the frequency range between 225 GHz and 255 GHz. The setup involves a digital Fast Fourier Transform Spectrometer (dFFTS) as backend. We determined important parameters of the receiver frontend such as the noise temperature, receiver antenna profiles and the Allan time. Finally, we demonstrated the capability of the system for heterodyne spectroscopy.

The paper is structured as follows: A short introduction of the receiver (RX) in section II is followed by the description of the experimental setups for the different characterization measurements and the respective results (section III). In section IV, we present the RX’s performance in our spectroscopy setup. We conclude with a summary and outlook in section V.

II. SYSTEM DESCRIPTION

The heterodyne RX was implemented in IHP’s SG13G2 technology, which is a $0.13 \mu\text{m}$ SiGe BiCMOS

technology with very high bipolar performance of $f_T/f_{max} = 300/500$ GHz. It consists of a $3.25 \text{ mm} \times 1.34 \text{ mm}$ RX chip with a bowtie-antenna. The chip is glued on the backside of a hyper-hemispherical silicon lens with 10 mm diameter and a 1.4 mm extension. Silicon was chosen due to the high refractive index (≈ 3.4) and low absorption (absorption coefficient $< 0.01 \text{ cm}^{-1}$ at 300 GHz). Simulations of the antenna directivity with the lens yield 3 dB beam widths of 6° and 7.3° in the E- and H-plane, respectively. The total efficiency of the antenna is $\approx 65\%$ (simulated for a transmitter (TX) with the same bowtie-antenna and silicon lens) [15]. The local oscillator (LO) of the RX is based on a voltage-controlled oscillator (VCO) which is tunable in frequency by an external phase-locked loop. The VCO signal is amplified and frequency-doubled before it reaches the mixer connected to the antenna, see Fig. 1. The mixer has a conversion gain of 13 dB [14]. The intermediate frequency (IF) is passed to a low-noise amplifier (LNA) and power detector or backend spectrometer through SMA-ports located on the baseband board. The circuit details of the RX are similar to the dual-band RX described in [15], but with only one frequency band. A metal plate is attached around the silicon lens for heat dissipation. The lens with the RX chip is mounted on an adapter board, which is plugged onto a baseband board (13 cm \times 13 cm including SMA ports) for evaluation purposes, see Fig. 1. The LO is tunable from 225 GHz to 255 GHz and the RX operates at room temperature. The power dissipation of board and chip is 3.3 W. For the chip alone, it is 0.93 W [15].

For spectrally resolved measurements, we used a digital Fast Fourier Transform Spectrometer (dFFTS) with 1.5 GHz bandwidth (DC to 1.5 GHz). It has 8192 spectral channels with 183 kHz width each [18].

III. RECEIVER CHARACTERIZATION

A. Antenna Profile

The setup for measuring cross-sections of the antenna profile was arranged as follows: The RX was mounted on a rotation stage and a TX which has the same design as the LO of the RX was placed in 50 cm distance to the RX. From our measurements described in [15], we can assume far-field conditions for this distance. The TX and the LO of the RX were set to a frequency of 241 GHz and 243.15 GHz, respectively. We detected the IF power with a diode power detector (Keysight 8472B), mounted behind a 200 MHz wide bandpass filter (Mini Circuits ZX75BP-2150-S+) and read out its voltage with a multimeter while rotating the RX around the vertical axis through its antenna. This was repeated with the TX and RX rotated by 90° around the optical axis, so that the cross-section of the antenna profile was measured both in the E- and H-plane.

The RX was turned in 1° steps in a 70° range to obtain an overview of the whole antenna profile (Fig. 2). Then the main antenna lobe was examined in 0.5° steps. We fitted a Gaussian function to the latter data. From that, we derived the far-field opening angles (full width at half maximum) which are $6.8^\circ \pm 0.2^\circ$ in the E-plane and $9.9^\circ \pm 0.1^\circ$ in the H-plane,

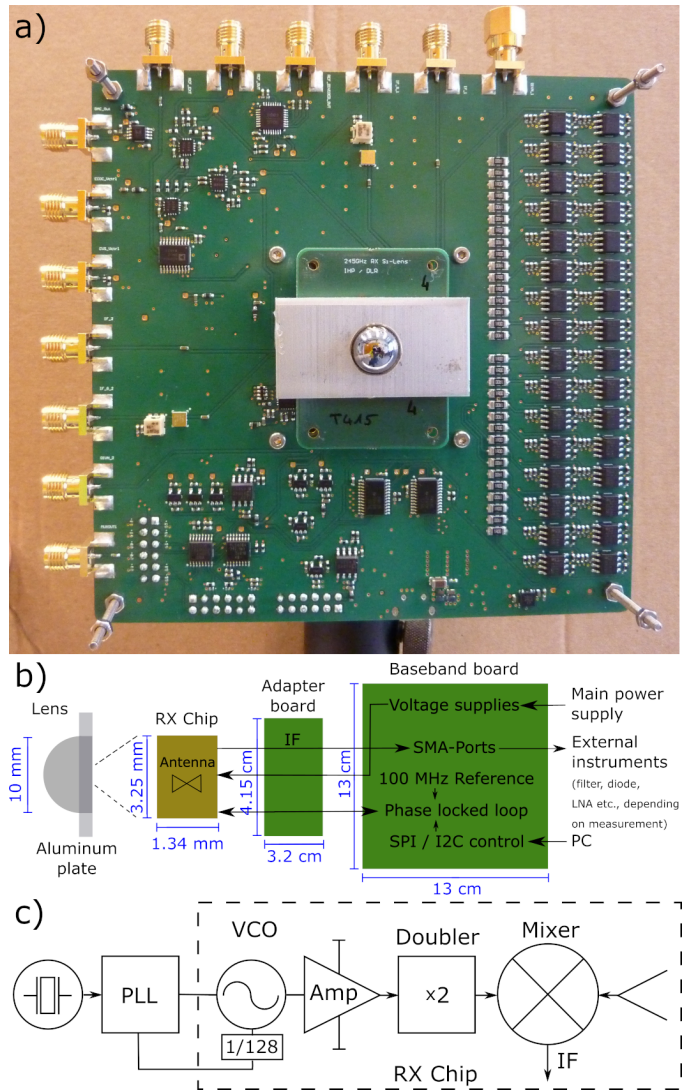


Fig. 1. a) Photograph of the heterodyne RX. The RX chip is on the backside of the 10-mm diameter silicon lens in the center of the adapter board which is mounted on a larger (13 cm \times 13 cm) evaluation board for the laboratory experiments. The lens is attached to a metal plate for heat dissipation. b) Schematic of the RX with dimensions and location of the different parts. c) Circuit diagram of the RX Chip and the external PLL.

respectively. The uncertainties denoted here originate from the covariance matrix of the fit. These results agree with the opening angles of the TX (6.2° and 9.9°) reported in [15], which operates at the same frequency and is equipped with the same bowtie antenna. The pronounced sidelobes in the E-plane antenna are caused by the bowtie antenna, which has noticeable sidelobes in the E-plane but not in the H-plane [15].

B. Noise Temperature

The noise temperature of the RX, T_{RX} , was determined with the Y-factor method. The RX was placed above a container lined with Eccosorb® and filled with liquid nitrogen. This served as cold load ($T_{cold} = 77$ K). It was covered with a piece of Eccosorb® at room temperature as hot load ($T_{hot} = 297$ K). The IF power was amplified (70 dB LNA chain, -10 dB at input), passed through a low-pass filter to

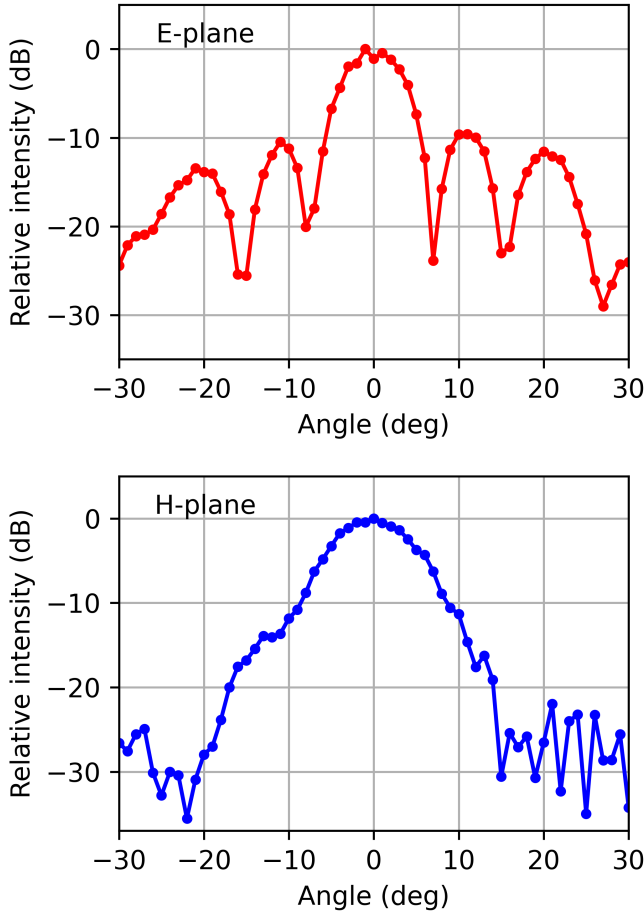


Fig. 2. Antenna profiles of the RX in the E-plane (top) and H-plane (bottom) as determined with a TX as source and a diode as power detector. The y-axis gives the relative intensity, referred to the intensity at the maximum. These measurements were performed at an RX frequency of 243.15 GHz.

avoid aliasing (DC to 1400 MHz), and then analyzed with the dFFTS. Additionally, a fan was used to reduce heating of the RX. From the IF spectrum across the whole IF bandwidth of 1.5 GHz, the double sideband (DSB) noise temperature was calculated according to

$$T_{RX} = \frac{T_{hot} - Y \cdot T_{cold}}{Y - 1} \quad (1)$$

with $Y = \frac{S_{hot}}{S_{cold}}$ and S_{hot} and S_{cold} being the signals from the hot and the cold load.

Fig. 3 shows the DSB noise temperature spectrum for an LO frequency of 240 GHz, which is in the center of the available frequency band. We removed 23 spikes (single data points) which originate from leakage of the divider signal for the PLL (LO frequency/256), the clock (100 MHz) and frequency mixing products thereof. The range around the divider signal (937.5 MHz), which is by far the most prominent disturbance, is marked in yellow. For the next RX generation, we will eliminate the spikes, for example by filtering. Frequencies up to 100 MHz are below the range of the amplifier chain, hence the calculated noise temperature increases at lower frequencies. This spectrum is the mean of 26 single noise temperature measurements. To better distinguish the level of

the noise temperature in the noise of the data, the mean of 10 spectral channels is displayed, resulting in a resolution of 1.83 MHz. The double sideband (DSB) noise temperature is between 10 000 K and 13 000 K (noise figure 15.4 dB - 16.5 dB) for this LO frequency.

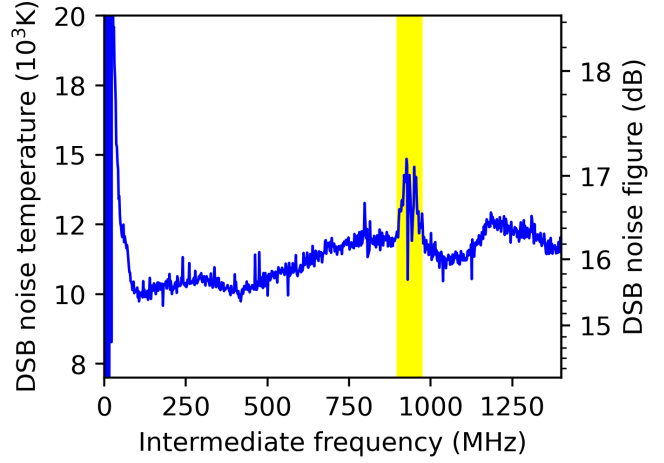


Fig. 3. Noise temperature of the RX for an LO frequency of 240 GHz. This dataset is the mean of 26 hot and cold measurements and the average of 10 spectral channels is displayed. Marked in yellow is the region around a parasitic divider signal (used for the PLL) which leaks to the IF port. The right axis displays the DSB noise figure.

From the root-mean-square (RMS) noise of the hot and cold spectra which lead to Fig. 3, we can estimate the minimum detectable temperature difference. For the mean of 26 spectra at 240 GHz with 1 s integration time each and 1.83 MHz spectral resolution, it is approximately 2 K (yielding $\approx 14 \text{ K s}^{1/2} \text{ MHz}^{1/2}$). This matches well with the radiometer equation, which yields 1.6 K for 11 000 K noise temperature for these parameters.

The DSB noise temperature was measured for different LO frequencies with an integration time of 1 s for one single spectrum. In Fig. 4, the mean of the noise temperature between 200 MHz and 400 MHz is shown for the different LO frequencies. The error bars represent the standard deviation of the datapoints used for the mean value. The DSB noise temperature is between 9 000 K and 20 000 K (noise figure 15.0 dB - 18.3 dB). This is lower than the values reported before ([15], [19]) because we use a fan to keep the RX at ambient temperature and due to some improvements of the setup, in particular with respect to the intermediate signal part. The noise temperature increases with the LO frequency. This might arise from the fact that the LO output power drops with increasing frequency as reported in [15]. These noise temperatures are well-suited for passive emission and absorption spectroscopy with moderate integration times.

C. Allan Time

To determine the Allan time of the RX, we placed a piece of room temperature Eccosorb® at a distance of 5 cm in front of the RX. We connected an amplifier (AFD4-010040-20P) to the IF port of the RX baseband board, followed by

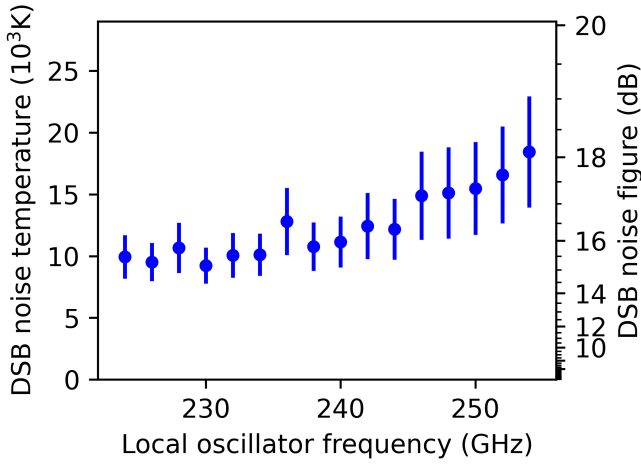


Fig. 4. DSB noise temperature of the RX for different LO frequencies. The data are the mean of the values for IF frequencies between 200 MHz and 400 MHz, the error bars represent the standard deviation in this range. The right axis shows the DSB noise figure.

a bandpass filter (Mini Circuits ZX75BP-2150-S+, 200 MHz wide), a power detector (Keysight 8472B), and a multimeter. We measured the power level of the IF signal for 10 min with a sampling rate of 1 kHz and an integration time of 1 ms.

Fig. 5 displays the Allan deviation for a LO frequency of 241 GHz in the interval between 1 ms and 10 s. The position of its minimum (Allan time) is between 1 s and 2 s. This Allan

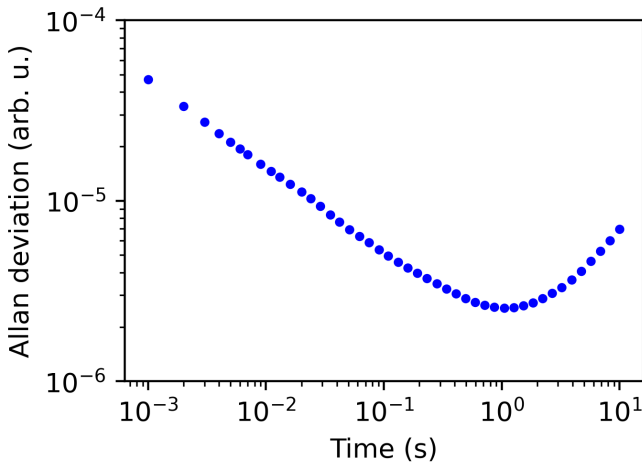


Fig. 5. Allan deviation as calculated from a 10 min measurement of the IF power. The LO was set to 241 GHz and the power level determined with a diode and a multimeter.

time enables the detection of spectral emission and absorption lines. In our setup, it is likely limited by environmental conditions such as temperature drifts and air perturbations since we used a fan to keep the RX temperature low. As the Allan time indicates the optimum averaging time [20], the results of these measurements were used as an orientation for the integration time of the spectra presented further on.

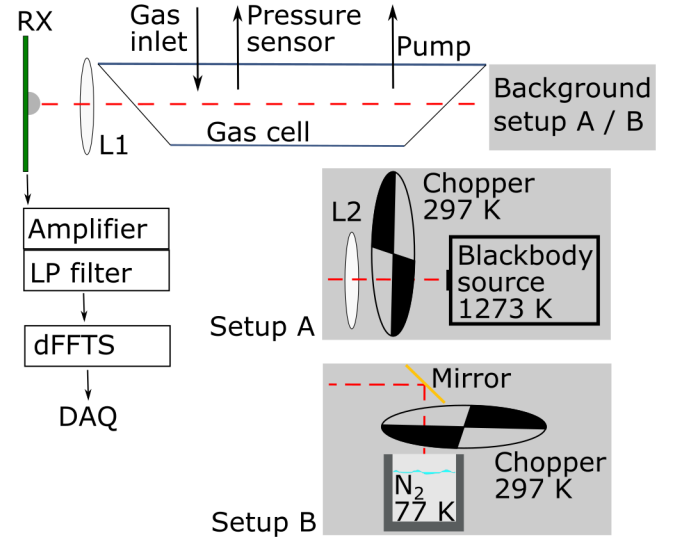


Fig. 6. Setup for heterodyne measurements of acetonitrile absorption (A) and emission (B) lines. The optical axis is marked in red.

IV. MOLECULAR SPECTROSCOPY

To demonstrate heterodyne spectroscopy with the RX, we chose acetonitrile (C_2H_3N) as a reference gas. It has multiple strong rotational transitions around 239 GHz. We chose to set the RX frequency to 239.3 GHz as this shifts all expected lines to the lower sideband. Two different experimental setups were used to measure absorption and emission spectra. The setup for absorption measurements (Setup A) is depicted in Fig. 6. A 65 cm long gas cell with Brewster windows made from high density polyethylene was placed between two polytetrafluoroethylene lenses ($f = 115$ mm). On one side, a black body source represented the hot background (1273 K). Its radiation was temporarily blocked by a chopper wheel whose surface (297 K) was the cold background. On the other side of the gas cell, the incoming radiation was detected with the RX. The IF signal was amplified by a 24-dB LNA (2.9 dB noise figure), filtered (LP filter DC to 1.4 GHz) and then analyzed with the dFFTS (183 kHz spectral resolution). For the measurement of emission spectra, we used Setup B (Fig. 6). An Eccosorb® lined container filled with liquid nitrogen served as cold background (77 K) and the chopper wheel surface (297 K) as hot background. One lens (L2) was replaced by a gold coated flat mirror.

For each setup, normalized emission and absorption spectra were determined from two sets of measurements: First, the evacuated gas cell was filled with acetonitrile and measurements were taken alternately with hot and cold background, 300 times each. Then, the gas cell was evacuated and the same procedure was repeated with the empty gas cell to obtain a reference spectrum. From the absorption measurements, the transmission τ was calculated according to

$$\tau = \frac{S_{hot,gas} - S_{cold,gas}}{S_{hot,empty} - S_{cold,empty}}. \quad (2)$$

Here, $S_{hot,gas}$ denotes the spectra taken with the gas-filled cell and the hot background, $S_{cold,gas}$ denotes the spectra

taken with the gas-filled cell and the cold background, and $S_{hot,empty}$ and $S_{cold,empty}$ are the according spectra with the empty gas cell. From the emission measurements, the normalized emission spectrum ϵ was calculated according to $\epsilon = 1 - \tau$.

Due to optical loss in the setup, the effective temperature T_{eff} seen by the RX differs from the physical load temperature T . The setup transmits a fraction t of the load emission and emits at room temperature (297 K). This leads to an effective load temperature of

$$T_{eff} = T \cdot t + 297 \text{ K} \cdot (1 - t). \quad (3)$$

We used the reference spectra without gas to calculate the effective noise temperature T_{setup} of the whole setup. From (1) and (3) we calculated the optical loss in the setup according to

$$t = \frac{T_{RX} + 297 \text{ K}}{T_{setup} + 297 \text{ K}}. \quad (4)$$

A. Absorption Spectroscopy

Fig. 7 shows different spectra ($S_{hot,gas}$, $S_{cold,gas}$, $S_{hot,empty}$, $S_{cold,empty}$) which were obtained with Setup A at 239.3 GHz LO frequency. The gas cell was filled with acetonitrile (30 Pa total pressure) and 300 single measurements with 1 s integration time were taken for each of the four spectra. The spectra are the mean of these measurements. In the hot spectrum, an acetonitrile absorption line at 275 MHz is visible as a dip.

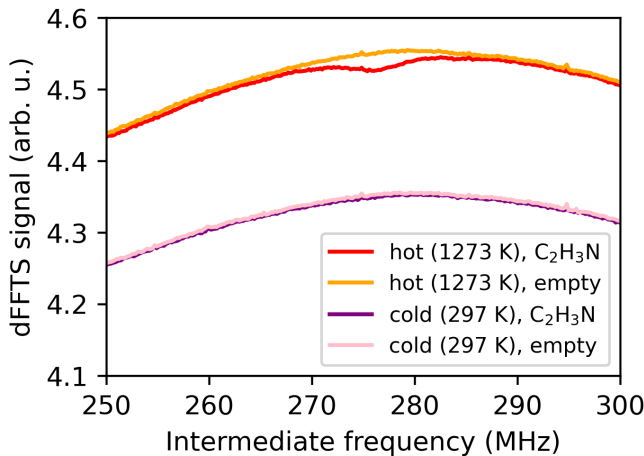


Fig. 7. Snippets from the spectra taken with Setup A to determine the acetonitrile transmission spectrum. The LO frequency was 239.3 GHz and for each spectrum 300 single measurements were taken with 1 s integration time. Spikes (single datapoints) were removed for this display. In the red spectrum, an absorption line is visible.

From the spectra with the empty gas cell, the effective DSB noise temperature of the setup was calculated to be $T_{setup} \approx 23\,000 \text{ K}$ between 200 MHz and 400 MHz. With a RX noise temperature of $T_{RX} = 11\,000 \text{ K}$ at this LO frequency (compare Fig. 4), the optical loss in the setup amounts to 52% according to (4). Approximately 23% loss is due to absorption and reflection at the two lenses and

two windows. Additional loss arises from the alignment and dimensions of the setup components: The antenna side lobes are partly outside the apertures of the optical components, as the far-field opening angle which includes the sidelobes is ≈ 4.5 times larger as the opening angle of the main antenna lobe only. With the different opening angles in E- and H-plane, the foci positions on the z-axis do not match and make the coupling to the small aperture (12.7 mm diameter) of the blackbody source difficult. Since the blackbody source is optimized for the infrared range, the emissivity in the millimeter wave range might be smaller than one. This leads to an additional overestimation of the loss when calculating it from the spectra.

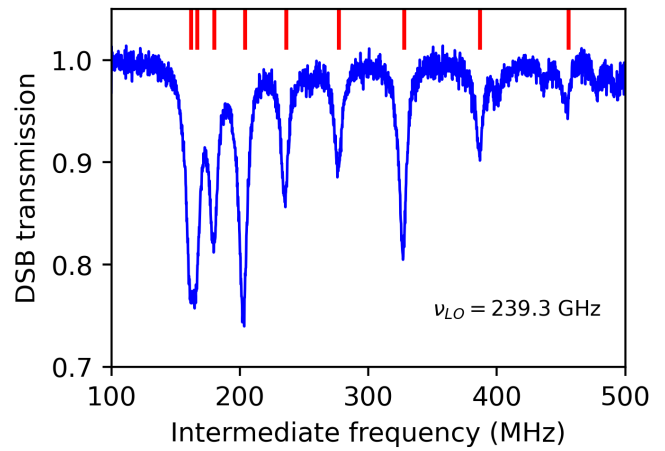


Fig. 8. DSB transmission spectrum of acetonitrile at a total pressure of 30 Pa for a LO frequency of 239.3 GHz. The spectrum is obtained as described by (2). The spectral resolution is 183 kHz. In red, the line positions from the JPL database are marked.

In Fig. 8, the transmission spectrum is shown, where the data are normalized as described by (2). The red sticks at the top indicate the line positions according to the JPL data base. These lines are all in the lower sideband of the RX. At this pressure, the first two lines appear as one broad line. Three additional weak lines which are not in the data base can be seen as well (at 260 MHz, 400 MHz, 450 MHz). They were also reported in a previous publication [21] and are detected in the upper sideband of the RX .

B. Emission Spectroscopy

With Setup B, we measured emission spectra of acetonitrile. Fig. 9 shows, analogous to Fig. 7, the mean of 300 spectra of measurements with hot (297 K) and cold (77 K) background, with and without gas in the cell. The LO frequency was 239.3 GHz and the total pressure 30 Pa. Here, the emission is visible as a peak in the spectrum with gas and cold background (dark blue). Note that the difference between the hot and cold signal is smaller than in Fig. 7, because of the smaller temperature difference between hot and cold background. In this setup, the noise temperature of the whole setup between 200 MHz and 400 MHz is $T_{setup} \approx 15\,000 \text{ K}$ (at 239.3 GHz LO frequency), which corresponds to an optical loss of 27%. Here, the two windows and the lens lead to approximately 12%

loss by reflection and absorption. The apertures of the optical components induce further loss, especially with regard to the antenna sidelobes as described for the absorption spectroscopy.

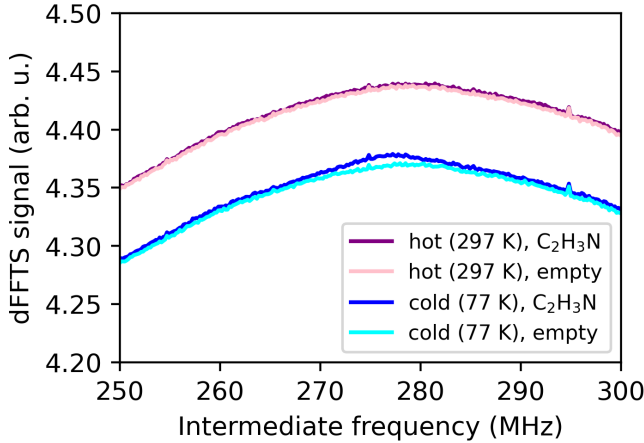


Fig. 9. Snippets from the spectra taken with Setup B to determine the acetonitrile emission spectrum. The LO frequency was 239.3 GHz and for each spectrum 300 single measurements were taken with 1 s integration time. Spikes (single datapoints) were removed for this display. An emission line is visible as peak in the dark blue spectrum.

In the DSB emission spectrum (Fig. 10), the same rotational transition lines as in Fig. 8 are visible, but the spectrum is noisier because of the smaller difference between the background temperatures.

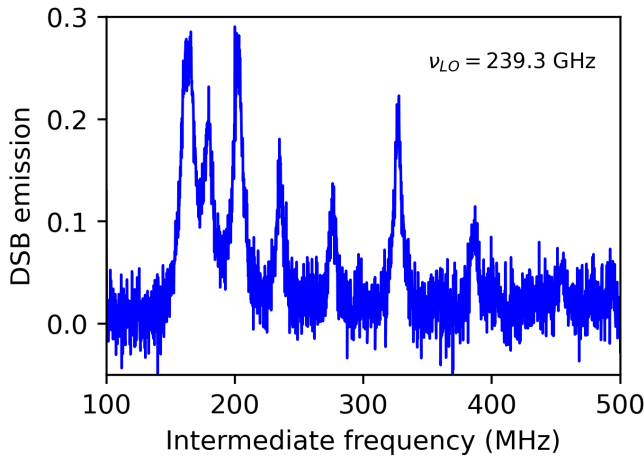


Fig. 10. DSB emission spectrum of acetonitrile at a total pressure of 30 Pa for a LO frequency of 239.3 GHz. The spectral resolution is 183 kHz.

Fig. 11 shows an emission spectrum at 10 Pa total pressure. Here, we applied a temperature scale (see description below) as y-axis to compare our spectrum with typical spectra of atmospheric gases. Due to the lower pressure, the line widths are a bit smaller than in Fig. 10. The figure shows a frequency range where only lines from the lower sideband appear.

We assumed a sideband ratio of 1. Measurements of the same emission line at different LO frequencies with the line one time in the upper and one time in the lower sideband confirmed this assumption. The spectrum was scaled to the

effective temperature range defined by the temperature of the loads and the optical loss of the setup. The RMS noise in the spectrum is 2.9 K and determines the brightness temperature of the weakest detectable lines in this setup with these parameters. The baseline here is considerably higher than typical baselines from atmospheric measurements. There, the cold background temperature is determined by the radiance from space and loss in the atmosphere whereas here, it is determined by the liquid nitrogen background (77 K) and the optical loss (4).

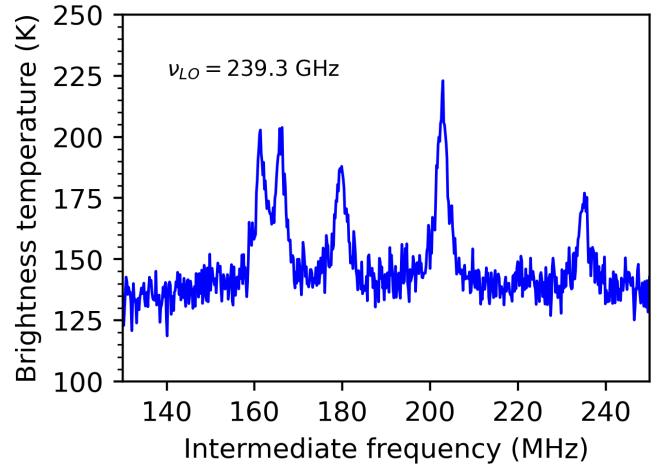


Fig. 11. Emission spectrum at 10 Pa acetonitrile, assuming a sideband ratio of 1. The y-axis represents the effective temperature scale considering the loss in the setup. The lines are from the lower sideband (LO frequency 239.3 GHz).

V. SUMMARY AND OUTLOOK

We characterized a RX fabricated in SiGe BiCMOS technology with regard to heterodyne spectroscopy. We demonstrated heterodyne absorption and emission spectroscopy in a laboratory environment. The results show that it is feasible to use the RX for heterodyne measurements in space, for instance for the examination of atmospheric gases. Key features of the RX are an Allan time of 1 s and a noise temperature between 9 000 K and 20 000 K for frequencies between 225 GHz and 255 GHz. The noise performance within the IF bandwidth between 0.1 GHz and 1.5 GHz varies only slightly from 11 000 K to 13 000 K at an LO frequency of 240 GHz. Noise temperatures of other heterodyne instruments for space applications which operate in this frequency range are e.g. 1 200 K – 1 600 K (DSB) for the 240 GHz radiometer of the EOS MLS [1]. This is smaller by about a factor of 10 than the noise temperature presented here. Still, with a minimum detectable temperature difference of approximately $14 \text{ K s}^{1/2} \text{ MHz}^{1/2}$, it seems feasible, for example by adjusting integration time and spectral resolution, to obtain spectra with a temperature resolution in the order of 1 K. Typical absorption lines of gases in the atmosphere have brightness temperatures from approximately 0.2 K up to several hundred Kelvin [1]. To achieve an RMS noise comparable to the one of the above-mentioned MLS radiometers (0.4 K for 96 MHz spectral channel width), the

integration time of our SiGe BiCMOS RX has to be about 15 s.

For measurements with a heterodyne spectrometer on a CubeSat, the spectroscopy setup would be reduced to RX, calibration load (for example a blackbody source), amplifier if necessary and spectrometer. As mentioned above, compact backend spectrometers for astronomical applications were already demonstrated [11], [17], [18].

An alternative approach to our SiGe RX is a hybrid CMOS / InP heterodyne spectrometer [17]. It features a horn antenna and an external InP LNA in front of the CMOS RX which has a center frequency of 183 GHz. The reported noise temperature varies between 700 K and 1000 K. This is roughly ten times better than our system which corresponds to 100 times shorter integration for the same SNR. Schottky diode mixers also achieve low noise temperatures. For example, in [22] the authors report on a 557 GHz GaAs membrane Schottky diode mixer with a DSB noise temperature of 1100 K. In [23], a 250 GHz Schottky diode mixer with DSB noise temperatures between 580 K and 1200 K is presented. Compared to InP and Schottky diode based RX systems, it is easier to produce a fully integrated RX system in SiGe BiCMOS technology. It offers a better integration into the baseband electronics and is available at lower cost. This is a significant advantage with respect to the application in small satellites.

The performance for spectroscopy can be further improved by optimizing the electronic circuitry in order to eliminate spurious signals, for example by appropriate filtering, and by improving the optics. Also, using a more advanced SiGe BiCMOS technology and cooling of the RX will result in a better noise temperature.

In conclusion, SiGe-based heterodyne receivers are promising for nanosatellite missions due to low costs and very good performance for passive gas spectroscopy and remote sensing.

REFERENCES

- [1] J. Waters, L. Froidevaux, R. Harwood, R. Jarnot, H. Pickett, W. Read, P. Siegel, R. Cofield, M. Filipiak, D. Flower, J. Holden, G. Lau, N. Livesey, G. Manney, H. Pumphrey, M. Santee, D. Wu, D. Cuddy, R. Lay, M. Loo, V. Perun, M. Schwartz, P. Stek, R. Thurstans, M. Boyles, K. Chandra, M. Chave, Gun-Shing Chen, B. Chudasama, R. Dodge, R. Fuller, M. Girard, J. Jiang, Yibo Jiang, B. Knosp, R. LaBelle, J. Lam, K. Lee, D. Miller, J. Oswald, N. Patel, D. Pukala, O. Quintero, D. Scaff, W. Van Snyder, M. Tope, P. Wagner, and M. Walch, "The Earth observing system microwave limb sounder (EOS MLS) on the Aura Satellite," *IEEE Transactions on Geoscience and Remote Sensing*, vol. 44, no. 5, pp. 1075–1092, May 2006.
- [2] K.-i. Kikuchi, T. Nishibori, S. Ochiai, H. Ozeki, Y. Irimajiri, Y. Kasai, M. Koike, T. Manabe, K. Mizukoshi, Y. Murayama, T. Nagahama, T. Sano, R. Sato, M. Seta, C. Takahashi, M. Takayanagi, H. Masuko, J. Inatani, M. Suzuki, and M. Shiotani, "Overview and early results of the Superconducting Submillimeter-Wave Limb-Emission Sounder (SMILES)," *Journal of Geophysical Research*, vol. 115, no. D23, p. D23306, Dec. 2010.
- [3] Y. J. Orsolini, J. Urban, D. P. Murtagh, S. Lossow, and V. Limpasuvan, "Descent from the polar mesosphere and anomalously high stratopause observed in 8 years of water vapor and temperature satellite observations by the Odin Sub-Millimeter Radiometer," *Journal of Geophysical Research*, vol. 115, no. D12, p. D12305, Jun. 2010.
- [4] H. Richter, C. Buchbender, R. Güsten, R. Higgins, B. Klein, J. Stutzki, H. Wiesemeyer, and H.-W. Hübers, "Direct measurements of atomic oxygen in the mesosphere and lower thermosphere using terahertz heterodyne spectroscopy," *Communications Earth & Environment*, vol. 2, no. 1, p. 19, Dec. 2021.
- [5] P. Hartogh, C. Jarchow, E. Lellouch, M. de Val-Borro, M. Rengel, R. Moreno, A. S. Medvedev, H. Sagawa, B. M. Swinyard, T. Cavalié, D. C. Lis, M. I. Błęcka, M. Banaszekiewicz, D. Bockelée-Morvan, J. Crovisier, T. Encrenaz, M. Küppers, L.-M. Lara, S. Szutowicz, B. Vandenbussche, F. Bensch, E. A. Bergin, F. Billebaud, N. Biver, G. A. Blake, J. A. D. L. Blommaert, J. Cernicharo, L. Decin, P. Encrenaz, H. Feuchtgruber, T. Fulton, T. de Graauw, E. Jehin, M. Kidger, R. Lorente, D. A. Naylor, G. Portyankina, M. Sánchez-Portal, R. Schieder, S. Sidher, N. Thomas, E. Verdugo, C. Waelkens, N. Whyborn, D. Teyssier, F. Helmich, P. Roelfsema, J. Stutzki, H. G. LeDuc, and J. A. Stern, "Herschel / HIFI observations of Mars: First detection of O₂ at submillimetre wavelengths and upper limits on HCl and H₂ O₂," *Astronomy and Astrophysics*, vol. 521, p. L49, Oct. 2010.
- [6] N. Biver, D. Bockelée-Morvan, J. Boissier, R. Moreno, J. Crovisier, D. C. Lis, P. Colom, M. A. Cordiner, S. N. Milam, N. X. Roth, B. P. Bonev, N. Dello Russo, R. J. Vervack, and M. A. DiSanti, "Molecular composition of comet 46P/Wirtanen from millimetre-wave spectroscopy," *Astronomy & Astrophysics*, vol. 648, p. A49, Apr. 2021.
- [7] R. Larsson, Y. Kasai, T. Kuroda, S. Sato, T. Yamada, H. Maezawa, Y. Hasegawa, T. Nishibori, S. Nakasuka, and P. Hartogh, "Mars submillimetre sensor on microsatellite: sensor feasibility study," *Geoscientific Instrumentation, Methods and Data Systems*, vol. 7, no. 4, pp. 331–341, Dec. 2018.
- [8] L. Rezac, P. Hartogh, R. Güsten, H. Wiesemeyer, H.-W. Hübers, C. Jarchow, H. Richter, B. Klein, and N. Honingh, "First detection of the 63 μm atomic oxygen line in the thermosphere of Mars with GREAT/SOFIA," *Astronomy & Astrophysics*, vol. 580, p. L10, Aug. 2015.
- [9] J. D. Liddle, A. P. Holt, S. J. Jason, K. A. O'Donnell, and E. J. Stevens, "Space science with CubeSats and nanosatellites," *Nature Astronomy*, vol. 4, no. 11, pp. 1026–1030, Nov. 2020.
- [10] N. M. Suhadis, "Statistical overview of CubeSat mission," in *Proc. AeroMech*, Penang, Malaysia, 2019, pp. 563–573.
- [11] Y. Zhang, Y. Kim, A. Tang, J. H. Kawamura, T. J. Reck, and M.-C. Frank Chang, "Integrated wide-band CMOS spectrometer systems for spaceborne telescopic sensing," *IEEE Transactions on Circuits and Systems I: Regular Papers*, vol. 66, no. 5, pp. 1863–1873, May 2019.
- [12] S. V. Thyagarajan, S. Kang, and A. M. Niknejad, "A 240 GHz fully integrated wideband QPSK receiver in 65 nm CMOS," *IEEE Journal of Solid-State Circuits*, vol. 50, no. 10, pp. 2268–2280, Oct. 2015.
- [13] C. Wang and R. Han, "Dual-terahertz-comb spectrometer on CMOS for rapid, wide-range gas detection with absolute specificity," *IEEE Journal of Solid-State Circuits*, vol. 52, no. 12, pp. 3361–3372, Dec. 2017.
- [14] M. H. Eissa, A. Awny, M. Ko, K. Schmalz, M. Elkhouly, A. Malignaggi, A. C. Ulusoy, and D. Kissinger, "A 220–275 GHz Direct-Conversion Receiver in 130-nm SiGe:C BiCMOS Technology," *IEEE Microwave and Wireless Components Letters*, vol. 27, no. 7, pp. 675–677, Jul. 2017.
- [15] K. Schmalz, N. Rothbart, A. Glück, M. H. Eissa, T. Mausolf, E. Turkmén, S. B. Yilmaz, and H.-W. Hübers, "Dual-band transmitter and receiver with bowtie-antenna in 0.13 μm SiGe BiCMOS for gas spectroscopy at 222 - 270 GHz," *IEEE Access*, vol. 9, pp. 124 805–124 816, 2021.
- [16] Z. Hu, C. Wang, and R. Han, "A 32-unit 240-GHz heterodyne receiver array in 65-nm CMOS with array-wide phase locking," *IEEE Journal of Solid-State Circuits*, vol. 54, no. 5, pp. 1216–1227, May 2019.
- [17] Y. Kim, Y. Zhang, T. James Reck, D. J. Nemchick, G. Chatopadhyay, B. Drouin, M.-C. Frank Chang, and A. Tang, "A 183-GHz InP/CMOS-hybrid heterodyne-spectrometer for spaceborne atmospheric remote sensing," *IEEE Transactions on Terahertz Science and Technology*, vol. 9, no. 3, pp. 313–334, May 2019.
- [18] B. Klein, I. Krämer, S. Hochgürtel, R. Güsten, A. Bell, K. Meyer, and V. Chetuk, "The next generation of fast Fourier transform spectrometer," in *Proc. 19th ISSST*, Groningen, The Netherlands, 2008, pp. 192–195.
- [19] A. Glück, K. Schmalz, N. Rothbart, and H.-W. Hübers, "Heterodyne spectroscopy with a 225 - 255 GHz SiGe BiCMOS receiver for space applications," in *2021 46th International Conference on Infrared, Millimeter and Terahertz Waves (IRMMW-THz)*, 2021, pp. 1–2.
- [20] P. Werle, R. Mücke, and F. Slemr, "The limits of signal averaging in atmospheric trace-gas monitoring by tunable diode-laser absorption spectroscopy (TDLAS)," *Applied Physics B Photophysics and Laser Chemistry*, vol. 57, no. 2, pp. 131–139, Aug. 1993.
- [21] P. F.-X. Neumaier, K. Schmalz, J. Borngreber, R. Wylde, and H.-W. Hübers, "Terahertz gas-phase spectroscopy: chemometrics for security and medical applications," *The Analyst*, vol. 140, no. 1, pp. 213–222, 2015.
- [22] H. Zhao, V. Drakinskiy, P. Sobis, J. Hanning, T. Bryllert, A.-Y. Tang, and J. Stake, "Development of a 557 GHz GaAs monolithic membrane-

diode mixer,” in *2012 International Conference on Indium Phosphide and Related Materials*, 2012, pp. 102–105.

- [23] Y. He, G. Liu, J. Zhou, K. Huang, J. Jiang, and W. Su, “340 and 250 GHz Schottky solid-state heterodyne receiver arrays for passive imaging systems,” *Microwave and Optical Technology Letters*, vol. 64, no. 6, pp. 1048–1055, 2022.



Alexandra Glück was born in Karlsruhe, Germany, in 1995. She received her B.Sc. degree in physics from University of Freiburg, Freiburg, Germany, in 2016 and her M.Sc. in physics from Humboldt-Universität zu Berlin, Berlin, Germany, in 2019. She is currently working towards her Dr. rer. nat. degree in physics at German Aerospace Center (DLR) in Berlin, Germany. Her work focuses on high resolution gas spectroscopy at GHz frequencies.



Heinz-Wilhelm Hübers received the Diploma and Doctoral degree in physics from the Universität Bonn, Bonn, Germany, in 1991 and 1994, respectively. From 1991 to 1994, he was with the Max-Planck Institut für Radioastronomie, Bonn, Germany. In 1994, he joined the Deutsches Zentrum für Luft und Raumfahrt (German Aerospace Center, DLR), Berlin, Germany, becoming the Head of Department in 2001. From 2009 to 2014, he has been a Professor of Experimental Physics with the Technische Universität Berlin, Berlin, Germany, and the Head of the Department “Experimental Planetary Physics,” DLR. In 2014, he became the Director of the Institute of Optical Sensor Systems, DLR, and a Professor with the Humboldt-Universität zu Berlin, Berlin, Germany. His research interests include THz physics and spectroscopy, particularly in THz systems for astronomy, planetary research, and security. Dr. Hübers was the recipient of the Innovation Award on Synchrotron Radiation in 2003, and the Lilienthal Award in 2007. In 2021, he received an honorary doctorate at Chalmers University of Technology, Gothenburg, Sweden.



Nick Rothbart was born in Berlin, Germany, in 1985 and received the Master of Science degree in physics from Humboldt-Universität zu Berlin in 2011. In 2015, he received the doctoral degree (Dr. rer. nat.) in physics from Technische Universität Berlin for his work on security-relevant terahertz imaging and spectroscopy. This work was accomplished at the German Aerospace Center (DLR) in Berlin and partly at the University of Massachusetts, Lowell, MA, USA, and was supported by a scholarship and a membership at the Helmholtz Research

School on Security Technologies (HRSST). From 2014 to 2015, he was also with the Federal Institute for Materials Research and Testing (BAM). Since 2015, he is involved in gas spectroscopy with Millimeter waves and Terahertz radiation at DLR and Humboldt-Universität zu Berlin.



Klaus Schmalz obtained his PhD in physics in 1978, and worked in the field of silicon semiconductor technologies and research for some time and has expertise in the area of thermally induced defects and characterization of Si/SiGe structures. After training in RF circuit design at UCLA in Los Angeles, 1998 - 1999, he changed his scientific focus to RF analog circuit design. Now, his research interest is the design of SiGe BiCMOS analog circuits for wireless communication with emphasis on RF front-ends for different standards and mm-wave circuits

for sensor applications. He has authored and co-authored more than 100 papers. K. Schmalz is currently with IHP, Frankfurt (Oder).